



Macroaggregated Albumin (MAA): Production, Size Optimization, Eu(III) and Tb(III) Complexes

Burcu UCAR^{1,*}   and Tayfun ACAR²  

¹Yildiz Technical University, Chemistry and Metallurgy Faculty, Department of Bioengineering, 34220, Istanbul, Turkey

Abstract: Herein, the synthesis of the macroaggregated albumin particles was carried out under different conditions for the size optimization that can be used in magnetic resonance, positron emission and fluorescence imaging. The size distribution analysis was performed with the Mastersizer and optimized MAA had 31.57 μm size and 0.36 PDI value. Morphological analysis was done with SEM. EDX and FT-IR analyzes were performed to study formed Eu^{3+} and Tb^{3+} complexes with optimized MAA. MAA complexes that can be used in lungs and liver imaging have been successfully obtained.

Keywords: MAA, Eu(III) complexes, Tb(III) complexes, Magnetic resonance imaging, Fluorescence imaging

Submitted: October 10, 2020. **Accepted:** December 23, 2020.

Cite this: Ucar B, Acar T. Macroaggregated Albumin (MAA): Production, Size Optimization, Eu(III) and Tb(III) Complexes. JOTCSA. 2021;8(1):209-16.

DOI: <https://doi.org/10.18596/jotcsa.808636>.

***Corresponding Author. E-mail:** brccr87@gmail.com, Telephone: +090-538-786-3200.

INTRODUCTION

Human serum albumin (HSA) is found in lymph, saliva, plasma (~60% of protein mass), cerebrospinal cord, and interstitial fluid. The secondary structure of HSA consists of 67% alpha-helix, 23% stretched chain, 10% beta-sheet, and folds. The change in the secondary and tertiary structures of HSA is due to the opening of this alpha-helical structure and the increase in beta-sheets. Protein aggregation occurs due to the partial opening of the tertiary structure and conformational changes of the secondary structure (1). The aggregation process of HSA consists of two steps: in the first step, as a result of the reversible nucleation occurring, proteins are thermodynamically incorporated in a reversibly growing nucleus sequentially. In the second step, after the

growing nucleus reaches a critical mass, protein molecules are added to the nucleus irreversibly. As a result, a large aggregate, which is very stable, is formed (1). In addition to the aggregation process, secondary structure changes occur due to the binding of metal complexes to a protein such as human serum albumin (HSA) (2).

Recently, some metal complexes bound to human serum albumin have shown high affinity toward DNA and have displayed various pharmacological properties (3). The development of metal complexes (especially Gallium, Gadolinium, and Lanthanides such as Europium and Terbium) that targeting cancerous cells under physiological conditions is of great current interest towards developing models for lots of pharmaceuticals from imaging

and contrast agents to metal-based radionuclide and chemotherapeutics agents (2, 4-6). These agents are of considerable interest as magnetic resonance imaging (MRI) agents, bioresponsive cellular imaging agents, luminescent bioprobes, and also in targeted radionuclide therapy before clinical application as simulating agents (2).

Terbium-149 (^{149}Tb), suggested as a potential alpha-emitter ($E_{\alpha} = 3.97 \text{ MeV}$; $I=17\%$) for targeted radionuclide therapy (TRT), has a relatively short half-life compared to ^{225}Ac , but four times longer than that of ^{213}Bi ($t_{1/2}$: 4.1 hours) and contains no daughter nuclides. ^{149}Tb can also be used in positron emission tomography (PET) of ^{149}Tb labeled radioligands, by reason of the co-emission of β^+ particles (positrons), and can be also stably coordinated with a DOTA chelator as a radiolanthanide. However, as it is assumed that ^{149}Tb is adsorbed on the surface of aggregates, there is no need to pre-conjugate the MAA with DOTA for labeling (7).

The PET or single-photon emission tomography (SPECT) tracer labeled MAA can accurately localize the tumor, determine the amount of perfusion, and provides better cross-sectional images for preoperative or pre-treatment planning, while providing intraoperative mapping through fluorescence or radioactive detection, using a hand probe or portable camera, and guides surgeons during tumor resection (8).

More than 80% of the administered albumin is retained in the pulmonary alveolar-capillary bed immediately after intravenous injection. Thus, the imaging procedure can be started immediately after injection. Since organ selectivity is a direct result of particle size, the sizes of labeled aggregates administered should be homogeneous and optimized. While aggregates below 1-10 micrometers are deposited by the reticuloendothelial system, aggregates above 10 micrometers are uptaken in the lung through a mechanical process. The erosion and fragmentation of the particles in the target organ reduced the particle size and thus, aggregates pass-through the pulmonary alveolar-capillary bed (9).

It is in the literature that MAA kits, which have been used in the clinic for radiolabeling with technetium-99m for many years, are used for labeling with metals such as lanthanides, gallium-68, and gadolinium (10). However, these kits are produced and optimized for labeling with technetium, so they contain many auxiliary substances that are not required for labeling with other metals. MAA, planned to be applied clinically in our study, was synthesized, optimized and labeled with relevant metals according to the purpose. This work forms the basis for manufacturing both a bioprobe, a contrast agent, and a radiotheranostic agent. The presented method and data will be used in the production of the agent to be applied in the mapping of liver and breast cancer, radio-guided occult lesion localization (11), and evaluation of regional perfusion in healthy and cancerous tissue.

We aim to prepare MAA particles that are sterile, free of pyrogens, with relatively long shelf-life, with a suitable range of particle size (30-80 μm) and higher radiochemical yields, showing diffusely increased tracer uptake in the lungs and liver.

MATERIAL AND METHODS

All reagents and solvents were commercial reagents of analytical grade and were used as received.

Production of the MAA Particles

0.4 or 0.8 mL of %20 HSA solution was diluted with 1 mL H_2O and 1.1 mL of %0.9 saline (NaCl). The obtained solution was sonicated in an ultrasonic bath (Bandeline) for 10 minutes or with a probe sonicator for a different time and amplitude. Then, 1 mL of %5 T80 was added to the HSA solution and the last volume was completed to 33.5 mL with 0.1M pH 5.8 PBS. The pH of the solution was controlled again. It is important that the pH is at the isoelectric point of HSA (pH 5.8-6.2). The mixture was stirred with a magnetic stirrer at 80 °C for 10 minutes. Next, it suddenly cooled to 25 °C. Heating and sudden cooling were performed twice (12, 13) and then it was lyophilized. Since the MAA obtained contains a large amount of salt, the salts were removed by washing and centrifugation three times and the MAA solution was lyophilized again.

Table 1: Synthesis parameters of the MAA particles.

	Amount of %20 HSA solution (mL)	Sonication Type	Sonication Conditions	T80
F1	0.4	Ultrasonic bath	10 min.	+
F2	0.4	Ultrasonic bath	10 min.	-
F3	0.4	Probe sonicator	30 sec., %50 W	+
F4	0.4	Probe sonicator	30 sec., %50 W	-
F5	0.4	Probe sonicator	45 sec., %50 W	-
F6	0.4	Probe sonicator	60 sec., %50 W	-
F7	0.4	Probe sonicator	45 sec., %60 W	-
F8	0.4	Probe sonicator	45 sec., %70 W	-
F9	0.8	Probe sonicator	45 sec., %50 W	-
F10	0.8	Probe sonicator	45 sec., %60 W	-
F11	0.4	Probe sonicator	45 sec., %60 W	-

Synthesis of Eu(III) and Tb(III) Complexes of the MAA Particles

5 mg of the MAA particles were dispersed in 1.5 mL of 1M AcONH₄ buffer solution at pH 4.8. 100 μ L of 4.11x10⁻⁵ M TbCl₃.6H₂O or 100 μ L of 5.35x10⁻⁵ M EuCl₃.6H₂O were added to 750 μ L of MAA solution. Complexing was carried out at 90°C at 300 rpm for 30 minutes. Washing was done in triplicate with 5 mL of 0.9% saline, and in triplicate with 5 mL dH₂O by centrifuge at 6000 rpm for 15 minutes. The excess metal remaining in the environment was removed. The complexes obtained were lyophilized and stored at -18 °C until reuse.

Size measurements of the MAA particles

The size distribution of the MAA particles was determined with Mastersizer (Hydro 2000MU, Malvern). After the production of the MAA particles, 10 mL of the emulsion was added to 250 mL of ultra-pure water until an obscuration rate of 5-15% was obtained. The samples were analyzed for the size distribution and particle size measurements were carried out in triplicate.

FT-IR Analysis of Eu(III) and Tb(III) Complexes of the MAA Particles

The molecular structure of the MAA, Eu(III)-MAA and Tb(III)-MAA were investigated by Fourier transform infrared (FT-IR) transmission spectra (IR-Prestige 21 FT-IR spectrophotometer, Shimadzu, Japan). MAA, Eu(III)-MAA, and Tb(III)-MAA were grounded into a fine powder. Then, the obtained powders were mixed with KBr powder and compacted into pellets for the FT-IR analysis. The spectra were examined in the wavenumber range of 400-4000 cm⁻¹ with a resolution of 4 cm⁻¹.

Scanning Electron Microscopy (SEM) Imaging and Energy dispersive X-Ray spectroscopy (EDX) Analysis

The surface morphology of the particles was viewed with scanning electron microscopy (SEM, EVO LS 10, Zeiss) with different magnification. To obtain SEM images, MAA particles were coated with a thin layer of Au-Pd at 10 mA for 60 seconds before observation (14).

Elemental analysis of Eu(III)-MAA and Tb(III)-MAA complexes were confirmed by EDX analysis.

RESULTS AND DISCUSSION

Size Distribution of the MAA Particles

MAA particles were produced in 11 formulations with different parameters (Table 1) to examine the effect of protein amount, stabilizer effect, sonication time and type on aggregate size. The size distribution and PDI values of the MAA particles were shown in Table 2. Size values of F1 and F2 formulations, made using ultrasonic bath, were found to be 191.75 and 131.91 microns, respectively. Due to the large size values, the sonication type was changed, and probe sonicator was used in other formulations. When T80 is used, it has been determined that the particle size is increased, and particles are obtained very far from the monodisperse, so no stabilizer was used in the F4-F12 formulations.

Subsequently, in the F4-F9 formulations, the power and duration of the probe sonicator were optimized. Three different times as 30, 45, and 60 seconds and three different powers 50, 60, and 70% watts were used. In the F4, F5, and F6 formulations, the size of the particles obtained with 50% watt power decreased from 59 microns to 16 microns by increasing the sonication time, but the PDI values were 0.3 for F4, 0.81 for F5 and 1.39 for F6. In other words, the increase in application time at constant power reduced the size and increased the PDI

values, causing the particles to have a polydisperse distribution.

Next, F7 (60% W) and F8 (70% W) was also produced at different sonication powers, together with the previously produced F5 (50% W). PDI values of 0.36 and 0.44 for F7 and F8, respectively, were accepted as monodispersed particles. The size of F7 was 31.57 microns, while F8 was measured as 14.13 microns. Finally, by varying the amount of HSA solution, F9 and F10 formulations were produced. While there was no significant difference in PDI values with the increase in protein amount, particle sizes increased by an average of 15-20 microns compared to F7. In line with these results, the F7 particles were determined as the optimized MAA particles. To show the reproducibility of this formulation, once again the F11 formulation was produced with the same parameters and its size was measured as 30.89 microns, and the PDI value as 0.43. F7 and F11 were consistent in size and PDI. The size distribution graph of the optimized MAA particles (F7) was given in Figure 1.

Table 2: The size distribution results of the MAA particles.

	Size (μm)	PDI
F1	191.75	0.42
F2	131.91	1.04
F3	56.12	0.37
F4	59.37	0.30
F5	34.28	0.81
F6	16.39	1.39
F7	31.57	0.36
F8	14.13	0.44
F9	44.83	0.38
F10	52.52	0.42
F11	30.89	0.43

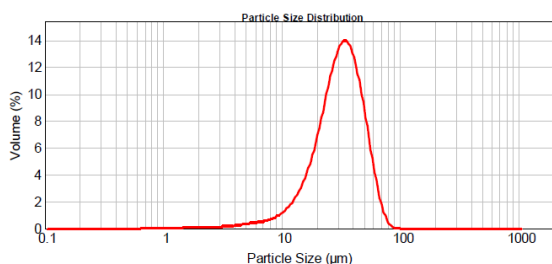


Figure 1: Size distribution graph of the optimized MAA particles (F7) (particle size distribution by volume).

Morphological Analysis of the MAA Particles

SEM images were taken from particles produced with the optimized formulation, F7. Morphological examination of F7 MAA particles was performed by SEM analysis as illustrated in Figure 2 and 3. SEM images confirmed the aggregation formation from the HSA. The images of aggregates taken at different magnifications were found to be compatible with the literature (15).

Synthesis of the Eu(III) and Tb(III) Complexes of the MAA Particles

Eu(III) and Tb(III) complexes of the F7 MAA particles were achieved. The complexes were analyzed by FT-IR and EDX.

FT-IR Analysis of the Eu(III) and Tb(III) Complexes of the MAA Particles

The Fourier Transform Infrared (FT-IR) analysis has been frequently applied for the recognition of organic and inorganic molecules. Figure 4 shows the FT-IR spectra of the Eu(III)-MAA and Tb(III)-MAA complexes comparatively with MAA. In the observed spectrum, the absorption bands of metal groups in the range of 500-700 cm^{-1} are clearly evident, differently from the MAA bands. Two sharp peaks of europium were seen at 534.7 and 621.7 cm^{-1} , while two sharp peaks for terbium at 626.9 and 533.6 cm^{-1} supported the presence of metals (16). A remarkable decrease in the peak intensities was determined in the spectra of the Eu(III)-MAA, and Tb(III)-MAA complexes, for the amide I band (1657.3 cm^{-1} , free MAA) and amide II band (1533.6 cm^{-1} , free MAA) area. It was thought that the decrease of the intensities was because of the interplay of metal ions with the C=O, C-N, and NH groups of HSA. The binding interactions between the MAA and the metal ions (Eu^{3+} and Tb^{3+}) were further evidenced by the spectral shifting of the amide I band from 1657.3 cm^{-1} in free MAA to 1651.8 cm^{-1} in the Eu(III)-MAA and 1651.4 cm^{-1} in the Tb(III)-MAA complexes. It has been noticed that the shift in this spectrum was due to the interplay of the Eu^{3+} and Tb^{3+} ions with the C=O and C-N groups of the MAA (17). In addition, a significant change was observed in the 1000-1200 cm^{-1} region. Unlike the spectrum of MAA, a double-headed broad peak appeared at 1076.0 and 1022.2 cm^{-1} for Eu(III)-MAA showed and at 1079.6 and 1024.4 cm^{-1} for Tb(III)-MAA. The changes in the three-dimensional structure of the aggregate due to the adsorption of the metal into the aggregate can be explained by the two vibration bands around 1075 and 1020 cm^{-1} of the threonine residue in the protein

structure (18, 19). These bands were compatible with the literature (20).

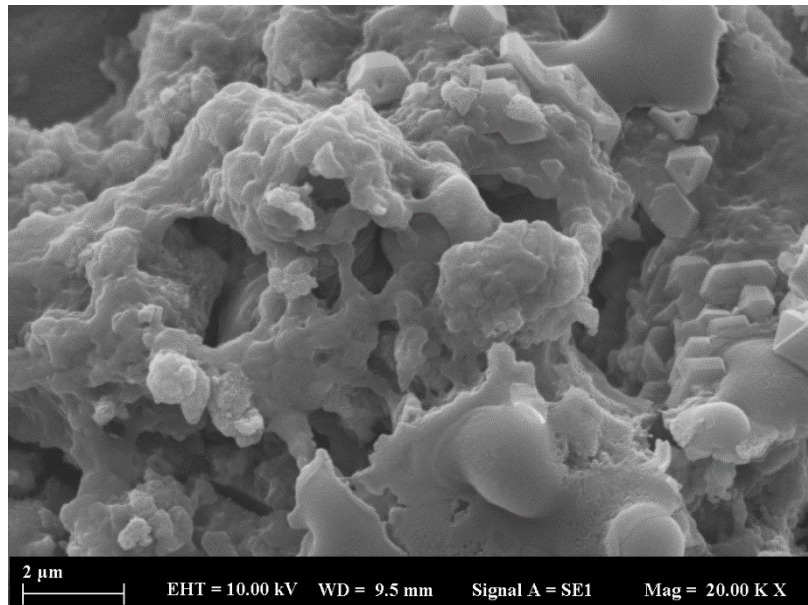


Figure 2: SEM image of the MAA particles (20.000).

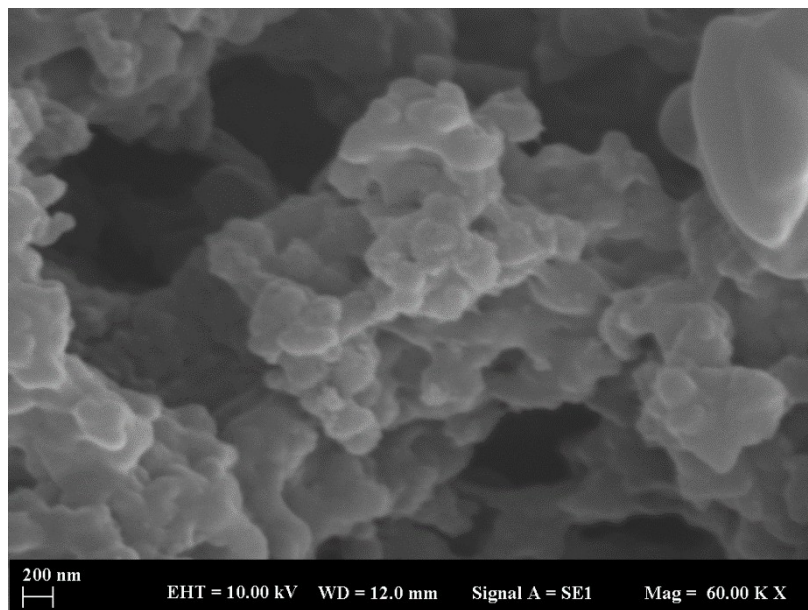


Figure 3: SEM image of the MAA particles (60.000).

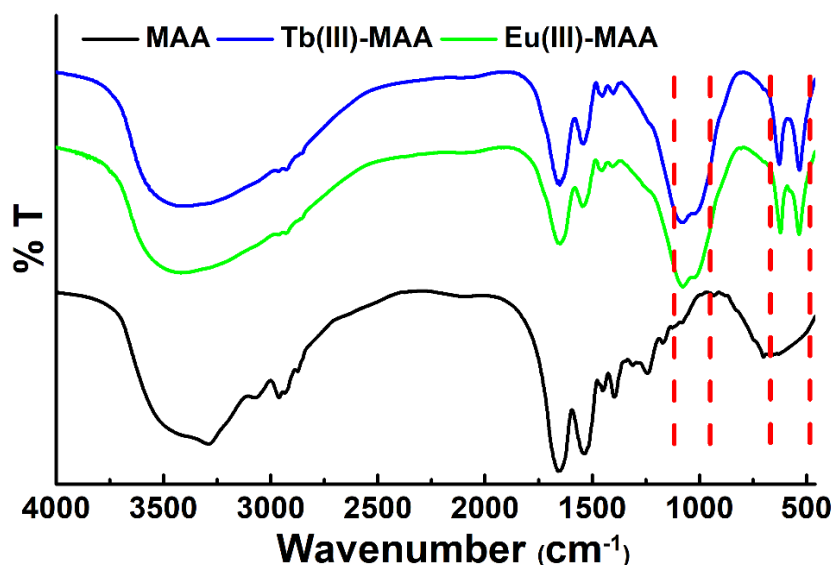
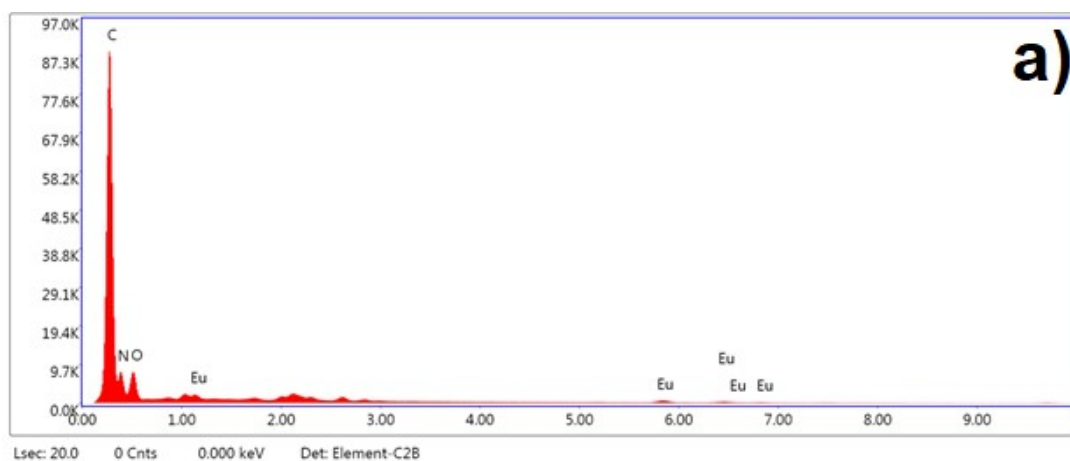


Figure 4: FT-IR spectra of the Eu(III)-MAA and Tb(III)-MAA complexes were given comparatively with MAA.

EDX Analysis of the Eu(III) and Tb(III) Complexes of the MAA Particles

EDX is a standard procedure for determining and measuring the fundamental composition of the area of samples from a few nanometers to micron size. The composition of the powder Eu(III)-MAA and Tb(III)-MAA samples were

measured using EDX. EDX spectra of the Eu(III)-MAA and Tb(III)-MAA complexes were given in Figure 5. The presence of Europium (Eu) and Terbium (Tb) in the resulting Eu(III)-MAA and Tb(III)-MAA complexes was evident in the corresponding EDX spectra in Figure 5a and 5b, respectively (21).



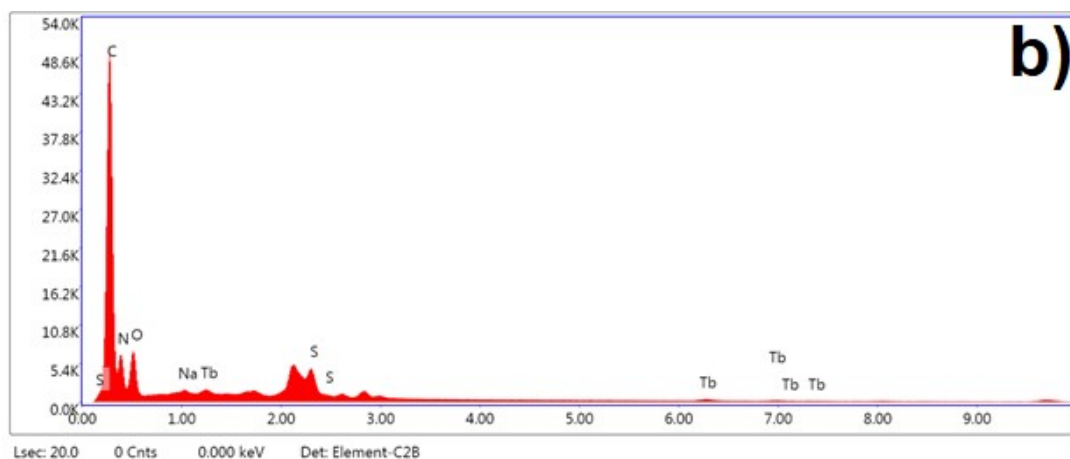


Figure 5: EDX spectra of the a) Eu(III)-MAA and b) Tb(III)-MAA complexes.

CONCLUSION

We have optimized the synthetic parameters of the MAA particles. Particles with an average size of 31 μm were chosen as optimized MAA. The structure of the metal complexes was evaluated by FT-IR analysis. The morphologies and qualitative analysis of the complexes were carried out using SEM-EDX. It is thought that the obtained Eu(III)-MAA and Tb(III)-MAA complexes can be used in magnetic resonance, positron emission and fluorescence imaging studies.

ACKNOWLEDGEMENT

The authors are grateful to Prof Dr. Tevfik Fikret CERMIK and Doç. Dr. Esra ARSLAN for critical revisions of the study. The authors also would like to thank M. Beşir ARVAS for all his support.

REFERENCES

1. Maciążek-Jurczyk M, Janas K, Pożycka J, Szkudlarek A, Rogóż W, Owczarzy A, et al. Human serum albumin aggregation/fibrillation and its abilities to drugs binding. *Molecules*. 2020;25(3):618.
2. Dasari S, Patra AK. Luminescent europium and terbium complexes of dipyridoquinoxaline and dipyridophenazine ligands as photosensitizing antennae: structures and biological perspectives. *Dalton Transactions*. 2015;44(46):19844-55.
3. Asadi Z, Mosallaei H, Sedaghat M, Yousefi R. Competitive binding affinity of two lanthanum (III) macrocycle complexes toward DNA and bovine serum albumin in water. *Journal of the Iranian Chemical Society*. 2017;14(11):2367-85.
4. Tikhonova TN, Shirshin EA, Budylin GS, Fadeev VV, Petrova GP. Assessment of the europium (III) binding sites on albumin using fluorescence spectroscopy. *The Journal of Physical Chemistry B*. 2014;118(24):6626-33.
5. Amor-Coarasa A, Milera A, Carvajal DA, McGoron AJ, editors. 99mTc-MAA vs. 68Ga-MAA as Perfusion Agents. 2013 29th Southern Biomedical Engineering Conference; 2013: IEEE.
6. Mathias CJ, Green MA. A convenient route to [68Ga] Ga-MAA for use as a particulate PET perfusion tracer. *Applied Radiation and Isotopes*. 2008;66(12):1910-2.
7. Umbricht CA, Köster U, Bernhardt P, Gracheva N, Johnston K, Schibli R, et al. Alpha-PET for Prostate Cancer: Preclinical investigation using 149 Tb-PSMA-617. *Scientific reports*. 2019;9(1):1-10.
8. Persico MG, Marengo M, De Matteis G, Manfrinato G, Cavenaghi G, Sgarella A, et al. 99mTc-68Ga-ICG-Labelled Macroaggregates and Nanocolloids of Human Serum Albumin: Synthesis Procedures of a Trimodal Imaging Agent Using Commercial Kits. *Contrast Media & Molecular Imaging*. 2020;2020.
9. MAA D. Kit for the Preparation of Technetium Tc 99m Albumin Aggregated Injection 2017 [Available from: <https://www.draximage.com/pdf/MAA-PI-Oct-2017-1.pdf>].
10. Mueller D, Kulkarni H, Baum RP, Odparlik A. Rapid Synthesis of 68Ga-labeled macroaggregated human serum albumin (MAA) for routine application in perfusion imaging

using PET/CT. *Applied Radiation and Isotopes*. 2017;122:72-7.

11. Dal F, Ökmen H, Yılmaz MK, Sarı S, Nazlı MA, Arslan E. Extraction of a foreign body from the breast using radio-guided occult lesion localization (ROLL): metallic foreign body in the breast. *European Journal of Breast Health*. 2017;13(3):159.

12. Al-Janabi M, Yousif Z, Kadim A, Al-Salem A. A new technique for the preparation of ready-to-use macroaggregated albumin (MAA) kits to be labelled with ^{99m}Tc for lung scanning. *The International journal of applied radiation and isotopes*. 1983;34(10):1473-8.

13. Ilyas M, Haider KH, Saeeda A, Javed M, Shams Z, Sameera C. In-House Preparation and Characterization of Ready-To-Use ^{99m}Tc-Sn-Macroaggregated Albumin Kit for Lung Perfusion Studies. *Medical Journal of Islamic Academy of Sciences*. 1998;11(4):131-8.

14. Arvas MB, Gorduk O, Gencten M, Sahin Y. Differential Pulse Voltammetric (DPV) Determination of Phosphomolybdenum Complexes by a Poly (Vinyl Chloride) Coated Molybdenum Blue Modified Pencil Graphite Electrode (PVC-MB-PGE). *Analytical Letters*. 2020:1-20.

15. Ament S, Maus S, Reber H, Buchholz H, Bausbacher N, Brochhausen C, et al. PET Lung Ventilation/Perfusion Imaging Using ⁶⁸Ga Aerosol (Galligas) and ⁶⁸Ga-Labeled Macroaggregated Albumin. *Theranostics, Gallium-68, and Other Radionuclides*: Springer; 2013. p. 395-423.

16. Maloubier M, Michel H, Solari PL, Moisy P, Tribalat M-A, Oberhaensli FR, et al. Speciation of americium in seawater and accumulation in the marine sponge *Aplysina cavernicola*. *Dalton Transactions*. 2015;44(47):20584-96.

17. Alhazmi HA. FT-IR spectroscopy for the identification of binding sites and measurements of the binding interactions of important metal ions with bovine serum albumin. *Scientia Pharmaceutica*. 2019;87(1):5.

18. Barth A. Infrared spectroscopy of proteins. *Biochimica et Biophysica Acta (BBA)-Bioenergetics*. 2007;1767(9):1073-101.

19. Liu X, Lee MJ, Coleman M, Rath P, Nilsson A, Fischer WB, et al. Detection of threonine structural changes upon formation of the M-intermediate of bacteriorhodopsin: evidence for assignment to Thr-89. *Biochimica et Biophysica Acta (BBA)-Bioenergetics*. 1998;1365(3):363-72.

20. Balamurugan A, Reddy M, Jayakannan M. Single polymer photosensitizer for Tb³⁺ and Eu³⁺ ions: An approach for white light emission based on carboxylic-functionalized poly (m-phenylenevinylene)s. *The Journal of Physical Chemistry B*. 2009;113(43):14128-38.

21. Dhanial SL, Chauhan A, Langyan R. Synthesis, characterization and photoluminescent properties of Eu (III) complexes with 5-hydroxy-2-hydroxymethyl-4H-4-pyranone and N, N'-donor heterocyclic coligands. *Rare Metals*. 2020:1-8.